Water Air Soil Pollut (2023) 234:324
https://doi.org/10.1007/s11270-023-06338-0

Reduction of Crystal Violet Dye from Water by Pomegranate Peel–Derived Efficient Biochar: Influencing Factors and Adsorption Behaviour

Noureddine Rouahna · Dhirar Ben Salem · Imane Bouchareb · Asma Nouioua · Abdelkader Ouakouak · Ammar Fadel · Noureddine Hamdi · Raj Boopathy

Received: 27 February 2023 / Accepted: 30 April 2023 / Published online: 10 May 2023

Abstract This work aimed to prepare a potential biochar from pomegranate peels (PP) and investigate its sorption ability toward a cationic dye, namely, crystal violet (CV). Adsorbent was obtained via a direct pyrolysis of precursor at 700 °C for 3 h. The biochar (PP-biochar) was characterized using FTIR, XPS, BET, SEM, and pH_{PZC} analysis, and used as adsorbent for the aqueous CV dye via batch experiments. Results showed that PP-biochar exhibits highly porous structure (S_{BET} = 508.9 m^2/g), V_T = 0.19 cm^3/g) with even distribution between micropore (50.8%) and mesopore (49.2 %) volume. The pH_{PZC} value of the prepared biochar was 6.42. The uptake of CV dye occurred rapidly, and the adsorbed amount reached 83.4% after only about 15 min of stirring time. It was also found that the adsorption kinetic mechanism was well described by the pseudo-second order and Avrami models. The maximum adsorption capacity of Langmuir (Q^0_{max}) was found to be 201.2 mg/g at 50 °C. Adsorption of CV dye involved mainly π-π interaction with contribution of other mechanisms (i.e., pore filling, hydrogen bonding, and electrostatic attraction). The finding suggest that the developed biochar is of promising potential to be applied as eco-friendly material for removing dyes from wastewater.

Keywords Pomegranate peel · Biochar · Bio-adsorbent · Crystal violet · Mechanism

1 Introduction

With the rapid evolution of industrial activities, large amounts of toxic pollutants including synthetic dyes are released into the aquatic environment. Most of

Supplementary Information The online version contains supplementary material available at https://doi.org/10.1007/s11270-023-06338-0.

N. Rouahna (✉) · A. Ouakouak
Faculty of Technology, University of El Oued, Box 789, 39000 El Oued, PO, Algeria
e-mail: rouahna2003@yahoo.fr

D. B. Salem · A. Nouioua
Research Laboratory in Subterranean and Surface Hydraulics, University of Biskra, Box 145, 07000 Biskra, PO, Algeria

I. Bouchareb
Laboratoire de Génie Mécanique et Matériaux, Université 20 Août 1955-Skikda, 26, 21000 Skikda, BP, Algeria

A. Fadel
Department of Industrial Chemistry, University of Biskra, Box 145, 07000 Biskra, PO, Algeria

N. Hamdi
Higher Institute of Sciences and Techniques of Waters, University of Gabès, 6072 Zrig, Tunisia

R. Boopathy
Department of Biological Sciences, Nicholls State University, Thibodaux, LA 70310, USA

these dyes are of synthetic origin and toxic in nature with suspected genotoxic and carcinogenic effects as well as low biodegradability (Cao et al., 2019). The textile industry releases wastewater containing toxic dyes, and around 2 to 20% is discharged directly into the environment as liquid effluents (Yaseen and Scholz, 2019). Crystal violet (CV) — a cationic dye — has a complex aromatic structure and can cause inhibitive effects on the photosynthesis of aquatic plants (Abu Elella et al., 2019). Therefore, it is crucial to treat CV dye-laden effluent prior to discharge. To date, several scholars have investigated the treatment of dye-contaminated waters by various techniques such as coagulation (Gasmi, Ibrahimi, et al., 2022), membrane separation (Khan et al., 2022), Fenton and photo-Fenton process (Guz et al., 2014), ion exchange (Bayramoglu et al., 2020), and electrocoagulation (Gasmi, Elboughdiri, et al., 2022). According to the literature, adsorption technique has been regarded as one of the most efficient methods for removing aqueous dyes even at high concentrations (Wu et al., 2020; Zbair et al., 2018). Among carbonaceous porous materials, in recent years, biochars are reported as low-cost and effective adsorbents for the removal of different types of aqueous pollutants (organic and inorganic). Biochars are prepared from pyrolysis of biomaterial source at high temperature and in the presence of little or no oxygen (Hu et al., 2020; Xiang et al., 2020). These carbon-rich materials have a good chemical stability, abundant functional groups, and advantageous textural characteristics (i.e., large specific surface area, high total pore volume) (Wu et al., 2020).

Moreover, biochar is environment-friendly and its preparation does not require chemical or physical activation like activated carbons (Chahinez et al., 2020). It is widely employed as adsorbent in plants of potable water and wastewater treatment (Vo et al., 2019).

In essence, biochar can be prepared by thermochemical decomposition of feedstock through several methods such as direct pyrolysis (Hadj-Otmane et al., 2022), hydrothermal carbonization (Vo et al., 2019), and gasification (Xiang et al., 2020). The physical and chemical characteristics of the resultant biochar are significantly affected by the thermochemical decomposition method and their conditions (i.e. temperature, duration, heating rate) as well as feedstock properties (Hadj-Otmane et al., 2022; Yu et al., 2019). In general, biochars can be developed through one-step (direct pyrolysis) or two-step process (hydrothermal carbonization followed by pyrolysis) (Tran et al., 2018; Vo et al., 2019).

In recent researches, efficient biochars were produced from available lignocellulosic wastes such as palm petioles (Hadj-Otmane et al., 2022), pepper stem (Naima et al., 2022), woody (Wathukarage et al., 2019), macroalgae (Sewu et al., 2019), and litchi peel (Wu et al., 2020).

In Algeria, especially in Biskra region, pomegranate farming produces a large amount of pomegranate peels (PP) annually. This biomass may serve as a good precursor for the production of biochar. Nevertheless, detailed investigations on the properties of PP-derived biochar (textural and structural characteristic, reuse, regeneration, feasibility) and adsorption mechanisms of cationic dyes are scarce in the existing literature. Therefore, the objective of this paper includes the following: (1) to investigate the characteristics of produced biochar, (2) to speculate the adsorption mechanism under different experimental conditions (i.e., pH, concentration, temperature, ionic strength), and (3) to examine the recycling performance and feasibility of the prepared adsorbent. The application of several kinetic and isotherm models was also investigated herein.

2 Materials and Methods

2.1 Materials and Reagents

Pomegranate peels (PP) was collected from Biskra region, Algeria (in November 2022). Crystal violet dye (type: cationic, chemical formula: $C_{25}H_{30}N_3Cl$, M_W: 408 g/mol, and solubility in water: 16 g/L at 25 °C) was purchased from Aldrich (USA) (Table S1). All chemicals used were of analytical grade, and all solutions were prepared using deionized water.

2.2 Preparation of Biochar

In this work, advantageous biochar with good level porosity was developed from pomegranate peels and used as potential adsorbent to eliminate aqueous CV dye. The starting material, pomegranate peels (PP), was cut into small pieces (≈ 0.5 cm) and washed with deionized water to remove dust and impurities, and

then dried at 80 °C for 48 h. The pyrolysis process of precursor was performed in one-stage under oxygen limited condition. The dried material was ground and sieved to sizes between 0.08 and 2 mm. Then, the selected powder was heated to 700 °C (with heating rate of 10 °C/min) for 3 h by using a covered crucible of porcelain. The temperature of 700 °C was selected because as reported in the literature at high values of temperature, the volatile organic compounds have been degraded and the obtained material consists mainly of carbon (Hadj-Otmane et al., 2022; Naima et al., 2022).

After pyrolysis, the obtained biochar was soaked in 0.1M of HCl solution, and then rinsed several times with deionized water until free of chloride in the filtrate. The obtained biochar (denoted as PP-biochar) was dried at 80 °C for 48 h and stored until further use.

2.3 Biochar Property

The biochar was synthetized via direct pyrolysis of precursor at 700 °C and characterized by different techniques (i.e., FTIR, SEM-EDS, XPS, BET, pH_{PZC}). The functional groups of adsorbent surfaces were investigated by the Fourier transform infrared spectroscopy (Shimadzu IR Affinity-1 Model, Tokyo, Japan). FTIR spectra were recorded in wave number range 400–4000 cm^{-1} with KBr disc method. Adsorption-desorption isotherm of nitrogen gas was measured at 77 K "Quantachrome instruments V11" and used to determine the textural properties of PP-biochar samples (i.e. BET surface area (S_{BET}), pore volume, and pore size). The XPS measurements were performed on a Kratos Axis Ultra using Alkα (1486.6 eV) radiation. High-resolution spectra were acquired at 20 eV pass energy with energy resolution of 0.9 eV. Surface morphology was inspected by scanning electron microscope (SEM) coupled by energy-dispersive X-ray spectroscopy (EDS) analysis "Tescan Vega 3." The pH of point zero charge of PP-biochar was determined according to protocol of the drift method as described by Aichour et al. (2019).

2.4 Batch Adsorption Experiments

The working solutions of CV dye were diluted from the stock solution with concentration of 500 mg/L. Adsorption experiments of CV dye onto PP-biochar were conducted using the common batch system. Approximately 50 mg of biochar was added into 100 mL Erlenmeyer flasks containing 50 mL of dye solution. The pH of the solution was adjusted by using 1 M NaOH or 1M HNO_3 before adding the biochar. The mixture (solid-liquid) was shaken at 150 rpm for the desired time (Hadj-Otmane et al., 2022). The separation of CV solution from the mixture dye-adsorbent was performed by filtration through 0.45 µm membrane. The residual concentration of CV dye in solutions was determined by UV–Vis spectrophotometer (Optizen 2120 UV) at λ_{max} = 590 nm which remains constant in pH range between 3 and 11 as shown in Fig. S1 (Pandian et al., 2015).

The relevant experiments such as adsorption kinetics (from 0 to 360 min), pH dependence (from 3.0 to 12), and ionic strength (from 0 to 1.0 M NaCl) were carried out at about 25 °C. The adsorption isotherm study (C_0 from 2 to 300 mg/L) was conducted at different temperatures (25 °C, 30 °C, and 50 °C) for 24 h. Each experiment was conducted in triplicate, and data were averaged.

2.5 Processing and Calculation of Data

The amounts of CV dye adsorbed onto biochar at every time (q_t; mg/g) and at equilibrium (q_e; mg/g) were calculated using equations of the mass balance (Eqs. 1 and 2, respectively) (Hadj-Otmane et al., 2022):

$$q_t = \frac{(C_o - C_t)}{m} V \tag{1}$$

$$q_e = \frac{(C_o - C_t)}{m} V \tag{2}$$

where C_o (mg/L), C_t (mg/L), and C_e (mg/L) are the concentrations of adsorbate at beginning, at time t, and at equilibrium; V (L) is the volume of CV dye solution; and m (g) is the used mass of biochar.

In this study, three common kinetic models and three adsorption isotherms were applied to explore the adsorption mechanisms. Details of such models have been provided by Lima et al., (2015) and Ouakouak et al., (2021). Equations of the pseudo-first-order (PFO), pseudo-second-order (PSO), and Avrami fractional-order models are given by Eqs. (3), (4), and (5), respectively (Table 1). Meanwhile, Langmuir,

Table 1 Equations and parameters of the used kinetic and isotherm models

Model	Equation	Parameters	Plot
PFO	$q_t = q_e\left(1 - e^{-K_1 t}\right)$ Eq. (3)	q_e and q_t (mg/g) are the adsorbed amount of CV dye at the end and at time t, respectively.	Fig. 7
PSO	$q_t = \frac{q_e^2.k_2.t}{1+q_e.k_2.t}$ Eq. (4)	K_1 (L/min) and K_2 (g/mg min) are the constants of PFO and PSO, respectively.	Fig. 7
Avrami	$q_t = qe \times \left(1 - e^{-(K_{AV} \times t)^{n_{AV}}}\right)$ Eq. (5)	k_{AV} (1/min) is the Avrami kinetic constant.	Fig. 7
		n_{AV} is a fractional order of adsorption.	
Langmuir	$q_e = \frac{Q^0_{\max}.K_L.C_e}{1+K_L.C_e}$ Eq. (6)	C_e is the concentration of CV dye at equilibrium.	Fig. 8
Freundlich	$q_e = K_F.C_e^{1/n_F}$ Eq. (7)	$Q^0_{\max}$ (mg/g) is the maximum capacity of the monolayer adsorption (of Langmuir).	Fig. 8
Redlich-Peterson	$q_e = \frac{K_{RP}.C_e}{1+a_{RP}.C_e^g}$ Eq. (8)	K_L (L/mg) is the constant of Langmuir isotherm.	Fig. 8
		K_F [(mg/g)/(mg/L)^n] is Freundlich constant.	
		n_F is the dimensionless parameter of intensity (of Freundlich).	
		K_{RP} (L/g) and a_{RP} (mg/L)$^{-g}$ are the constants of Redlich-Peterson isotherm.	
		g_{RP} the dimensionless exponent of Redlich-Peterson, g should be ≤ 1.	

Freundlich, and Redlich–Peterson isotherm are provided by Eqs. 6, 7, and 8, respectively. The non-linear regression of the abovementioned models was investigated using functions in the Origin software.

The best-fitted model representing the mechanism of CV dye adsorption onto the PP-biochar was reflected by calculating the correlation (R^2), standard deviation (SD), and chi-square (χ^2) value as follow (Lima et al., 2019):

$$R^2 = 1 - \frac{\sum \left(q_{e,\exp} - q_{e,\mathrm{cal}}\right)^2}{\sum \left(q_{e,\exp} - q_{e,\mathrm{mean}}\right)^2} \quad (9)$$

$$SD = \sqrt{\left(\frac{1}{n-p}\right) \times \left[\sum_{i=1}^{n} \left(q_{e,\exp} - q_{e,\mathrm{cal}}\right)^2\right]} \quad (10)$$

$$\chi^2 = \sum \frac{\left(q_{e,\exp} - q_{e,\mathrm{cal}}\right)^2}{q_{e,\mathrm{cal}}} \quad (11)$$

where $q_{e,\mathrm{mean}}$ (mg/g) is the average of q_e experimental values; n is the number of point in the test; p is the number of parameters in the used equation. The best suitable equation is for the highest R^2, but the smaller SD and χ^2 values.

2.6 Reusability and Regeneration of PP-Biochar

The objective of the laden biochar reuse is to minimize the cost of the operation and reduce the quantities of resulting wastes. In this study, several adsorption cycles (reuse), desorption, and regeneration tests were conducted (Rouahna et al., 2018). The PP-biochars (0.2 g) were added into 200 mL of dye solution (C_0 = 30 mg/L) and stirred for 4 h. The laden biochar was collected and dried for the next test. When the percentage of elimination of CV dye decreased

less than 50%, the recovered adsorbent was washed with 0.1 M solution of HCl under vigorous stirring to release the adsorbed molecules of dye. Then, the material was washed with distilled water, and was dried to use in new adsorption experiment (regeneration). The percentage of CV dye removed from water is determined as follows:

$$\textit{Removal}\ (\%) = \left(C_0 - C_e\right)/C_0 \times 100 \quad (12)$$

3 Results and discussions

3.1 Property of PP-Biochar

FTIR spectra of PP-biochar samples (native and laden adsorbent) are presented in Fig. 1. The intense band appeared at 3436 cm^{-1} is assigned to the elongation vibrations of the -OH groups, which characterize the functional groups of the carboxylic acids and alcohols (Wu et al., 2020). Peaks observed at 2924 and 2852 cm^{-1} are attributed to the asymmetric and symmetrical stretching vibrations of C-H binding (Cunha et al., 2020). Vibrations obtained at 1740 and 1631 cm^{-1} indicate the presence of C=O of carboxylic groups and C=C in aromatic ring, respectively (Tomul et al., 2019). Peak at 1420 cm^{-1} denotes the ionic carboxylic groups (-COO^{-}) (Naima et al., 2022). The intense peak at around 1115 cm^{-1} represent the C-O vibrations (Tran et al., 2017). Lastly, the narrow peak at 618 cm^{-1} indicates the vibrations of C-H bond of aromatic rings (Grimm et al., 2022). Moreover, the new peaks observed at 1051 and 573 cm^{-1} confirm the characteristic vibrations of dye molecules fixed on the laden biochar surface.

Figure 2 shows the morphology and main components (obtained by EDS) of biochar surface. As observed, the analysed sample exhibits heterogenous structure with tunnel form of pores. The high porosity of material was created by the pyrolysis of lignin and cellulose of the biochar structure (Changmai et al., 2018).

The chemical composition of PP-biochar surface was investigated by the XPS analysis technique as depicted in Fig. 3. The spectrum of survey scan indicated that the analyzed material had a high content of carbon (88.13%; Fig. 3a) (Chahinez et al., 2020). In addition, the presence of oxygen (11.13%) confirms that the external biochar surface possesses groups containing oxygen. Moreover, the deconvolution of C1s spectra depicted in Fig. 3b show three components based on the principle of C element (Mao et al., 2017). Peak at the binding energy of 284.6 eV was assigned to the aliphatic and aromatic C structures (C-H, C-C, and C=C). The peak observed at

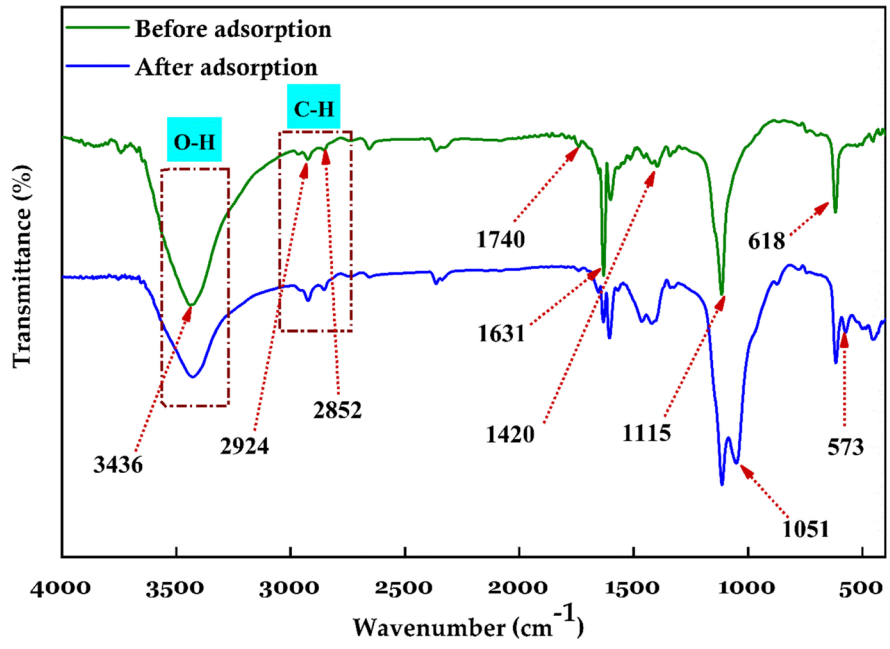

Fig. 1 FTIR spectra of PP-biochar before and after adsorption tests

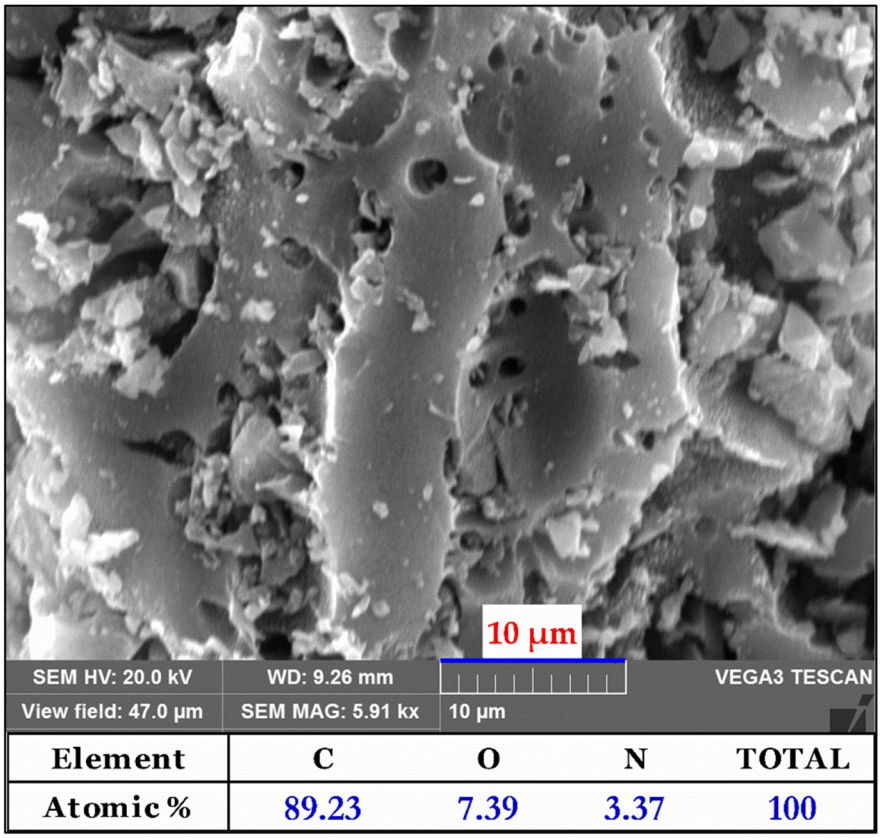

Element	C	O	N	TOTAL
Atomic %	89.23	7.39	3.37	100

Fig. 2 SEM image and EDS of PP-biochar surface

285.6 eV characterizes the C-O binding of alcoholic and phenolic structures. Similarly, the O1s spectrum confirms also that the PP-biochar has un important fraction of oxygen-rich functional groups at the B.E of 530.9 eV (C=(O, N, metal)), 531.5 eV (C=O), and 532.8 eV (C-O) as shown in Fig. 3c (Liu et al., 2020; Tran et al., 2020). Furthermore, the existence of N element is confirmed by the EDS (%, Fig. 2) and the XPS (0.62 %, Fig. 3a) analysis which suggests the presence of -NH_2 groups at the material surface (Msaadi et al., 2022).

Figure 4 depicts the isotherm adsorption/desorption of N_2 for the PP700-biochar sample. This isotherm belongs to category I according to IUPAC nomenclature. Such type is characteristic of microporous adsorbent (average pore diameter < 2.0 nm) with less contributions of external surface area. Additionally, the N_2 isotherm showed a hysteresis loop of H_4-type at high values of pressure (Boakye et al., 2019). The external surface (S_{ext}, m^2/g) and volume of micropores (V_{Micro}, cm^3/g) were calculated using the t-plot method as demonstrated in previous works (Naima et al., 2022; Tran et al., 2018). Results show that the prepared biochar possesses a good surface area (S_{BET} = 508.9 m^2/g). The total volume of pores was accounted for 0.193 cm^3/g with almost even distribution between micropore (50.8%) and mesopore (49.2 %). Additionally, the external fraction of surface area and average diameter of pores were found to be 171.7 m^2/g and 1.52 nm, respectively. The microporous characteristic of PP-biochar sample was confirmed also by value of the characteristic energy of adsorption which was found to be 18.51 16 kJ/mol (excessed 16 kJ/mol) according to Dubinin-Radushkevich equation (Eq. 13) (Sevilla et al., 2011):

$$E_0 = \frac{10.8}{L_0} + 11.4 \tag{13}$$

where L_0 (nm) represents the average diameter of pores.

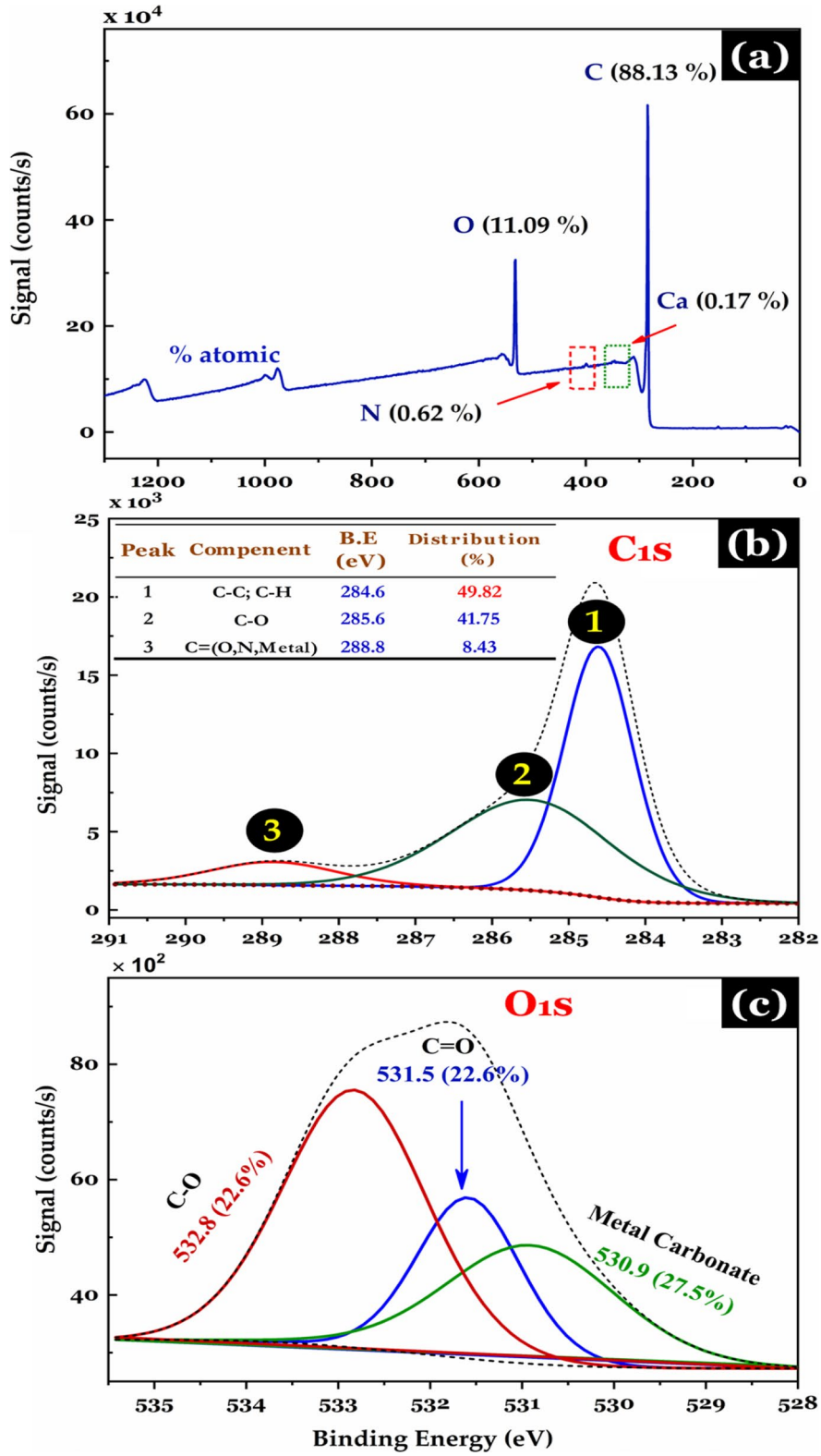

Fig. 3 XPS analysis for PP-biochar: **a** the survey scan spectrum and the high-resolution scans of **b** C 1s and **c** O 1s (the peak assignments for each spectrum are depicted in the legend)

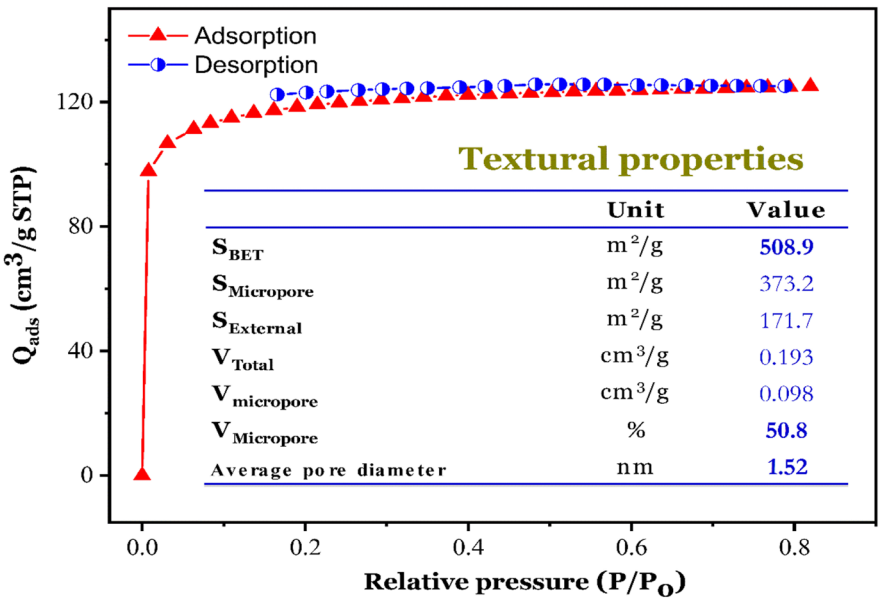

Fig. 4 Adsorption/desorption isotherm of N_2 gas of PP-biochar at 77 K

3.2 Adsorption Ability and Mechanisms

Crystal violet is a pH-sensitive dye known as a pH indicator due to its colour changes in an acidic or basic medium (Sabnis, 2007). Likewise, previous research reported the significant role of pH factor on CV dye adsorption from water (Chahinez et al., 2020; Ouakouak et al., 2021).

Figure 5a depicts that the adsorption capacity of PP-biochar slightly increased with the augmentation of solution pH from 3 to 12. A matching outcome was reported in a study by Chahinez et al. (2020). The point of zero charge of PP-biochar (pH_{PZC} ≈ 6.4) is critical in determining the adsorption capacity (Fig. 5b). At this value of pH, the biochar surface is neutral and does not have a net charge. At pH values

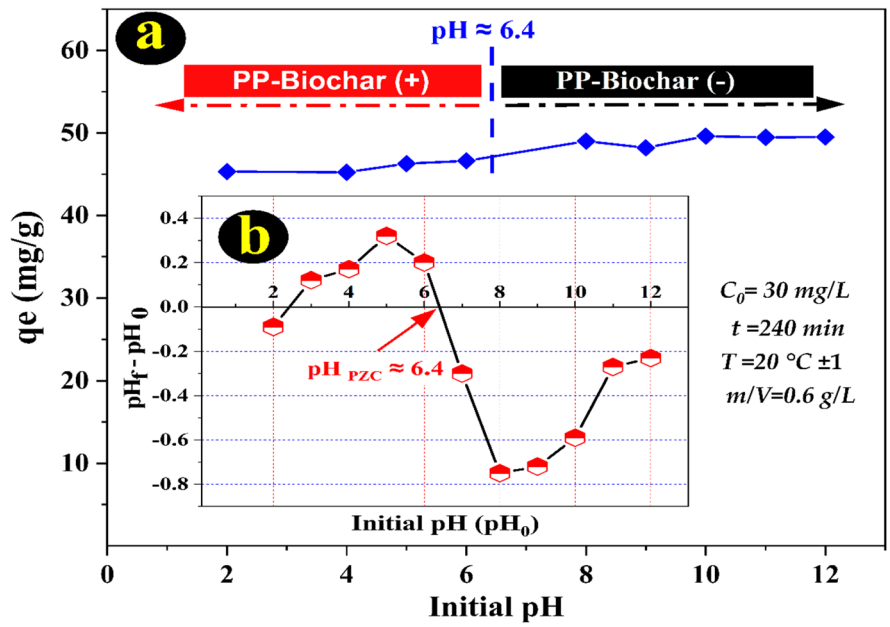

Fig. 5 The influence of pH on the adsorption process (**a**) and the pH_{PZC} property of PP-biochar (**b**)

below 6.4, the biochar surface was positively charged and repelled the positively charged crystal violet ions due to the formed positively charged species hydroxyl ion ($–OH_2^+$) and ammonium ion ($–NH_3^+$), limiting the adsorption capacity. However, as the pH increased above 6.4, the adsorbent surface became more negatively charged, which attracted the positively charged CV ions and slightly increased the amount of the adsorbed dye. Thus, this development explored a mechanism known as an electrostatic attraction but has a weak contribution to the adsorption process (Tran et al., 2017).

Figure 6 a reveals that the adsorbed CV dye onto PP-biochar is not significantly affected by changing NaCl concentrations from 0.1 to 1 M. In the absence of sodium chloride, the adsorption quantity (q_e) value was about 47 mg/g; subsequently, this value was weakly subsided and rested almost stable at around 46 mg/g when the NaCl increased from 0.1 to 1 M. Hence, the non-effect of sodium chloride on the adsorption process confirmed again that electrostatic attraction between the dye and biochar surface is a negligible mechanism.

It is also possible that π-π interaction mechanism may involve a combination in the adsorption process. To investigate it, modified PP-biochar by oxidation by HNO_3 was compared to PP-biochar in removal efficiency (Fig. 6b). As expected, the PP-biochar has a higher adsorption capacity compared to oxidized biochar, regardless of the initial concentration of the target substance, and this could be because the oxidation process may have altered the surface properties of the PP-biochar, reduced the number of aromatic rings in the presence of oxygen groups, thus reducing the potential interactions between the π-electrons in the surface groups of adsorbent and the π-electrons in the aromatic ring of CV dye (Coughlin and Ezra, 1968). Consequently, the π-π interaction mechanism is mainly responsible for CV dye adsorption. This observation was also confirmed by the decrease of C=C bond intensity in the FTIR spectrum after adsorption (Huff and Lee, 2016). On the other hand, the high adsorption capacity at a pH near the pH_{PZC} suggests the existence of contributed mechanisms like pore-filling based on the porosity and the large specific surface area of the PP-biochar or the presence hydrogen bonding interaction (Tran et al., 2017).

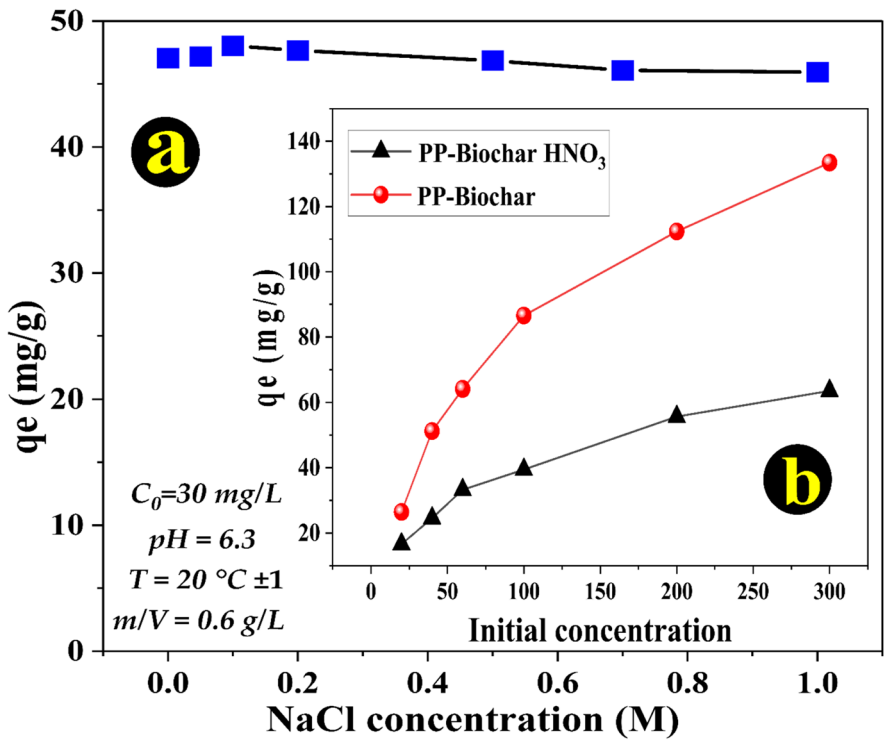

Fig. 6 The ionic strength effect on the adsorption capacity (a) and comparison between PP-biochar and oxidized PP-biochar in CV removal (b).

3.3 Kinetic Study

Figure 7 shows the quantity of the CV dye adsorbed (Q_t) onto PP-biochar over time (0 to 360 min) and the calculated parameters by modelling the kinetic data using the above-mentioned models (Table 2). From the results, it appears that the adsorption process occurred rapidly in the first minutes, with 40.23 mg/g adsorbed amount of dye obtained within 5 min. This can reflect the high affinity of PP-biochar towards the CV dye molecules. The equilibrium of adsorption was attained after nearly 60 min of stirring time, and the adsorption rate remains almost stable until the end as the adsorbent seems saturated.

Furthermore, the ability to quickly reach an equilibrium state with effective removal in the operation is a critical consideration in selecting materials for water treatment on an industrial scale.

It was also found that the Avrami and pseudo-second-order models provide the best fit to the experimental data, followed by pseudo-first-order model based on the highest values of R^2 and the lowest values of SD and χ^2 errors.

Table 2 Parameter values obtained by modelling the kinetic data

Model	Unit	Value	Standard error
Pseudo-first-order			
q_e	mg/g	43.95	0.343
k_1	L/min	0.462	0.059
R^2	—	0.987	—
SD	—	1.26	—
χ^2	—	1.59	—
Pseudo-second-order			
q_e	mg/g	44.72	0.220
k_2	g/mg min	0.031	0.004
R^2	—	0.996	—
SD	—	0.67	—
χ^2	—	0.45	—
Avrami			
q_e	mg/g	45.49	0.622
k_{AV}	1/min	9.893	9.053
n_{AV}	—	0.190	0.047
R^2	—	0.998	—
SD	—	0.50	—
χ^2	—	0.25	—

3.4 Adsorption Isotherm

In this study, the adsorption of CV dye onto PP-biochar was studied at several initial concentrations of dye (from 2 to 300 mg/L), at fixed solid/liquid ratio (0.6 g/L), and at three different temperatures (20 °C, 30 °C, and 50 °C) as shown in Fig. 8. The equilibrium

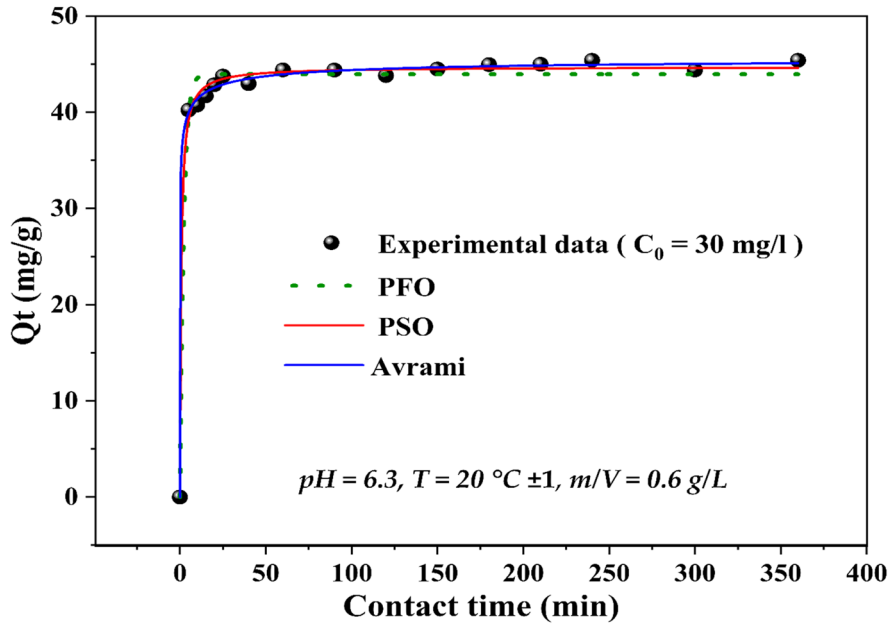

Fig. 7 Stirring time factor effect on CV dye uptake by PP-biochar

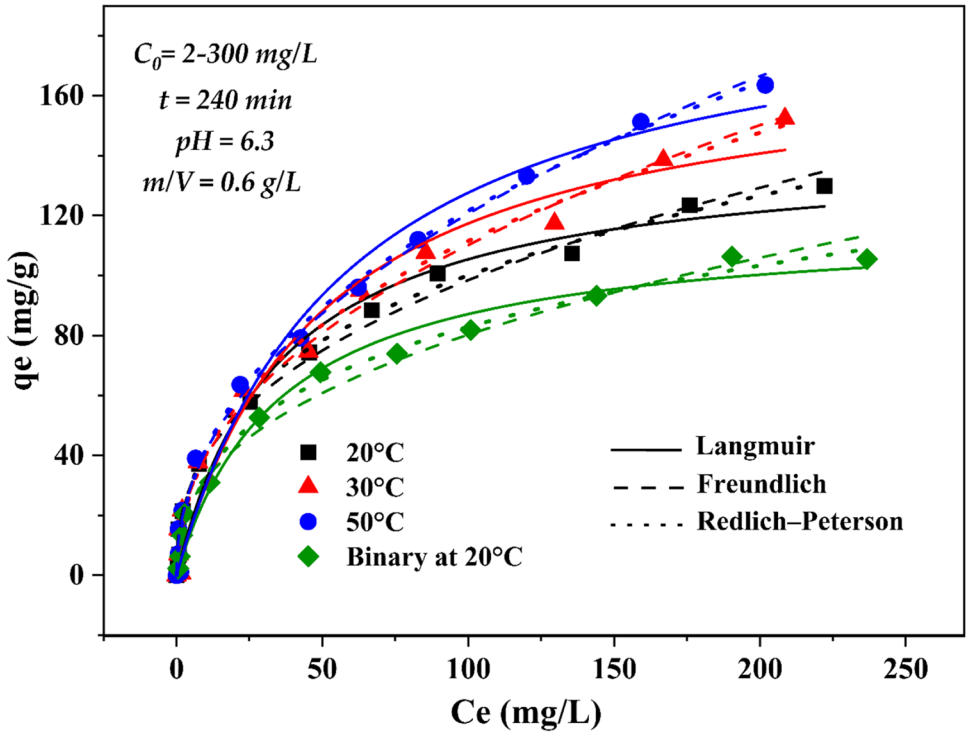

Fig. 8 Modelling isotherm data of CV dye adsorbed by PP-biochar

data were then modelled to predict the best isotherm model for describing the adsorption system and provides information concerning the equilibrium behaviour (capacity and mechanism).

As expected, at low initial concentrations (2, 5, 10, 15, and 30 mg/L), the results showed that the adsorbent has a high affinity toward CV molecules based on the removal efficiency (R%) ranging from 91.4 to 99%. Furthermore, adsorption equilibrium data were described by the three selective models. In detail, the higher non-linear R^2 values (0.982–0.995) and lower both SD (3.29–6.35) and χ^2 (10.85–40.41) values indicated that the Redlich-Peterson and Freundlich models were more suitable for describing the adsorption isotherm compared to the Langmuir model in the individual mode or the presence of 60 mg/L of MB dye (Table 3).

Additionally, the dramatic uptake of CV dye with increased temperature was expressed by the increase in the maximum adsorption capacity of the PP-biochar at higher temperatures. The Langmuir Q^0_{max} values were calculated to be 142.7 mg/g (20 °C), 175.7 mg/g (30 °C), and 201.2 (50 °C) in the single mode. It also found that adding MB — a cationic — dye in the solution reduced the adsorption capacity of the CV dye to 118.07 mg/g at 20 °C despite the biochar still having excellent affinity to dye. Thus, there exists a competition effect between CV and MB onto the PP-biochar surface, that is, because the MB molecules can be adsorbed by the biochar via the similar mechanisms (i.e., π-π interactions, pore filling, electrostatic attraction, H-bonding) as the CV dye molecules. According to this results, it can be concluded the designed biochar could serve as a valuable material in cationic dye remediation even in the presence of several competitive dyes.

3.5 Reusability Study

One of the important factors to consider when using biochar is its reusability, as it affects the overall cost-effectiveness of the treatment process. Therefore, the experiment was designed to explore the capacity of the PP-biochar in adsorbing 30 mg/L by regenerating many times and then reusing the materials after the desorption test (Fig. 9).

Table 3 Parameter values obtained by modelling the isotherm data

Model	Unit	Value (by mode and temperature)			
		20 °C	20 °C	30 °C	50 °C
		Single	binary	Single	Single
Langmuir					
$Q^0{}_{max}$	mg/g	142.66	118.07	175.69	201.17
K_L	L/mg	0.028	0.028	0.020	0.017
R^2	—	0.976	0.980	0.971	0.974
SD	—	7.66	5.75	9.60	9.84
χ^2	—	58.72	33.08	92.28	96.89
Freundlich					
n	—	2.54	2.49	2.23	2.15
K_F	$(mg/g)/(mg/L)^n$	16.14	12.69	14.08	14.17
R^2	—	0.991	0.982	0.987	0.991
SD	—	4.74	5.32	6.35	5.59
χ^2		22.51	28.40	40.41	31.28
Redlich-Peterson	L/g				
K_{rp}	$(mg/L)^{-g}$	23.98	10.13	21.73	29.00
a_{rp}	—	0.987	0.389	1.054	1.534
g	—	0.683	0.729	0.621	0.586
R^2	—	0.995	0.994	0.989	0.992
SD	—	3.39	3.29	6.07	5.44
χ^2		11.54	10.85	36.90	29.62

The results from the regeneration adsorption revealed a gradual decrease in the removal efficiency over multiple cycles. In the first cycle, the removal efficiency was recorded at 96.28%, but it dropped to 44.24% in the fourth cycle. This decrease in adsorption efficiency can be attributed to the continuous exhaustion of the active sites on the surface of the adsorbent.

The desorption quantity of about 69.87 mg/L represents 82.74% of the total adsorbed dye onto biochar in the regeneration test (84.43 mg/L), indicating that a considerable amount of CV molecules could be recovered from materials using the HCl agent (1M) after the adsorption process.

After reusing the PP-biochar, the removal efficiency was kept high at 88.48% despite being slightly lower than the removal efficiency obtained in the first cycle, which confirmed the desorption finding. These features of PP-biochar can further reduce the overall cost of the process and make it a practical technique for industrial applications.

3.6 Comparison with Other Biochars

To support the ability of the PP-biochar as a potential adsorbent for the removal of dyes from water media, the textural properties of PP-biochar and the estimated value of theoretical adsorption capacity ($Q^0{}_{max}$) were compared to results of various biochars that have been reported by other scholars in the existing literature. Results in Table 4 show that the PP-biochar samples have a high surface area, pore size distribution and high total pore volume compared to other biochars that investigated in other works. In addition, data of Table 4 confirm that the produced biochar in this work (PP-biochar) exhibited an excellent adsorption capacity towards CV dye (175.7 mg/g at 30 °C) compared to other kinds of biochars (11.0–206.6 mg/g) which reported in the previous studies.

3.7 Cost Analysis

The cost analysis of biochar production is critical to determine its economic feasibility in marketing and different applications. In general, biochar production requires guaranteeing the availability of raw materials and covering the net cost of production, including feedstock purchase cost, energy consumption cost, transport cost, and labour cost (Ahmed et al., 2016). Some operating expenses like the raw feedstock and the energy could lower by using free sources such as agricultural waste and sunlight power. In addition, the operation of the biochar production is simple and did not need advanced technology or many workers. Accordingly, the total cost of producing PP-biochar (C_{total}) was analysed and estimated based on the Algeria prices (converted to US$) as the following :

$$C_{Total} = C_{\text{Feedstock}} + C_{\text{Production}} + C_{\text{Additional}} \quad (14)$$

where the cost of production ($C_{\text{Production}}$) represents the energy (electricity) consumption cost for drying and oven heating; and the additional cost ($C_{\text{Additional}}$) covers the use of water in the process including the need for washing and transporting costs. The total cost for producing 1 kg of PP-biochar was calculated to be 0.343 US$ in the condition of labour. From this finding, the cost of the prepared biochar is

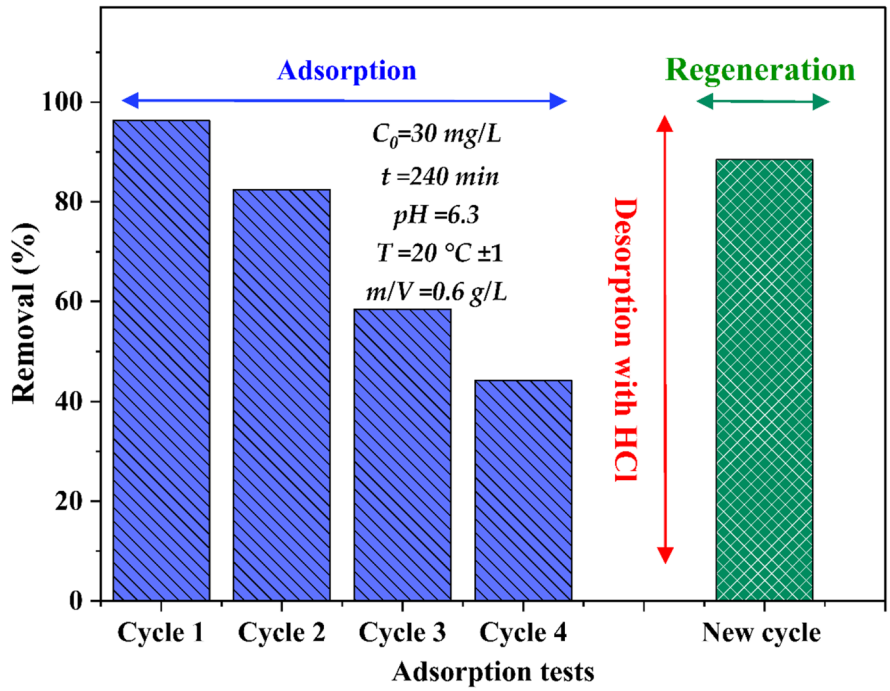

Fig. 9 Adsorption cycles, desorption, and reusability of PP-biochar

Table 4 Comparison of the adsorption capacity (Q^0_{max}) of dyes onto PP-biochar with other biochars reported in the literature

Kind of biochar	Porosity		Experimental conditions of adsorption isotherm					Q^0_{max} (mg/g)	Ref.
	S_{BET} (m^2g)	V_{toal} (cm^3/g)	*Dye*	pH	*m/V* (g/L)	C_o range (mg/L)	*T* (°C)		
Palm Petioles biochar (at 700 °C)	640.0	0.403	CV	7.0	1	5–250	20	196.5	Chahinez et al. (2020)
Rice straw biochar (at 500 °C)	104.0	-	CV	7.0	0.6	-	25	44.6	Abd-Elhamid et al. (2020)
Woody biochar (at 300 °C)	1.0	0.001	CV	8.0	2	5–200	30	11.0	Wathukarage et al. (2019)
Woody biochar (at 500 °C)	76.3	0.01	CV	8.0	2	5–200	30	23.7	
Woody biochar (at 700 °C)	808.0	0.89	CV	8.0	2	5–200	30	125.5	
Corncob biochar (at 500 °C)	33.7	--	CV	-	2	25–200	25	81.9	Fang (2012)
Palm Petioles biochar (at 600 °C)	430.4	0.22	MB	7.0	1	2–500	20	118.7	Hadj-Otmane et al. (2022)
Palm Fronds biochar (at 700 °C)	431.8	0.13	MB	-	-	20–200	25	206.6	Zubair et al. (2020)
PP-biochar (at 700 °C)	508.9	0.19	CV	6.3	1	2–300	30	175.7	This study

Rt room temperature, *CV* crystal violet, *MB* methylene blue

Table 5 Comparison of costs between PP-biochar and other materials

Material	Price (US$)	Quantity	Net cost (US$)	Total cost (US$/kg)	Reference
PP-biochar				0.343	This study
PP feedstock	0.01/kg	5	0.025		
Deionized water	0.05/L	4	0.2		
Energy	0.011/kWh	6.2	0.068		
Transporting			0.05		
Activated carbon (granular)				6.4	Alhashimi and Aktas (2017)
Virgin wood biochar				17.8	Alhashimi and Aktas (2017)
Coconut shell biochar				0.55	Praveen et al. (2021)
Eggshell-modified biochar				0.33	Kumi et al. (2020)
Activated charcoal*				0.85–2.85	https://www.alibaba.com
Rice straw biochar				0.55	Sakhiya et al. (2022)
Tectona grand biochar				0.432	Pandit et al. (2018)
Teff straw activated biochar				3.50	Yihunu et al. (2019)

*Commercial prices in 2023

comparable to that of other carbonaceous materials, as shown in Table 5.

Based on the calculation of Table 5 and the reusability study, the cost of 1 m^3 of treated water is about 0.206 US$ without regeneration and 0.051 US$ with regeneration (after 4 cycles of reuse) for m/V = 0.6 g/L, C_0 = 30 mg/L, pH ≈ 6.3, and T ≈ 20 °C. Therefore, the PP-biochar could be considered a low-cost adsorbent for marketing and large-scale applications.

4 Conclusion

In this study, the performance of biochar prepared from pomegranate peels in eliminating crystal violet (CV) from the water was successfully investigated under various conditions. The adsorption ability of CV molecules was not affected by solution pH (3–12) or ionic strength (0.1 to 1M NaCl), confirming the insignificant role of the electrostatic attraction mechanism. Modifying the pomegranate peel biochar with HNO_3 resulted in a significant decrease in the amount of CV adsorbed compared with PP-biochar, proving the primary role of the π-π interactions mechanism. The high CV uptake near the pH_{PZC} confirmed the presence of pore-filling and hydrogen bonding interaction as minor mechanisms. The experimental data were best represented by the Avrami and pseudo-second-order models. The Redlich-Peterson and Freundlich models are very suitable in describing the adsorption isotherm. Modelling using the Langmuir isotherm estimated the maximum adsorption capacity to be 142.7 mg/g (20°C), 175.7 mg/g (30°C), and 201.2 (50°C). The PP-biochar showed the capacity for four adsorption cycles before being reused. The findings indicate the potential use of pomegranate peel biochar as a low-cost and alternative material in environmental applications.

Data Availability The datasets generated during and/or analysed during the current study are available from the corresponding author on reasonable request.

Declarations

Conflict of Interest The authors declare no competing interests.

References

Abd-Elhamid, A. I., Emran, M., El-Sadek, M. H., El-Shanshory, A. A., Soliman, H. M. A., Akl, M. A., & Rashad, M. (2020). Enhanced removal of cationic dye by eco-friendly activated biochar derived from rice straw. *Applied Water Science, 10*(1), 45. https://doi.org/10.1007/s13201-019-1128-0

Abu Elella, M. H., Sabaa, M. W., ElHafeez, E. A., & Mohamed, R. R. (2019). Crystal violet dye removal using crosslinked grafted xanthan gum. *International Journal of Biological Macromolecules, 137*, 1086–1101. https://doi.org/10.1016/j.ijbiomac.2019.06.243

Ahmed, M. B., Zhou, J. L., Ngo, H. H., & Guo, W. (2016). Insight into biochar properties and its cost analysis. *Biomass and Bioenergy, 84*, 76–86. https://doi.org/10.1016/j.biombioe.2015.11.002

Aichour, A., Zaghouane-Boudiaf, H., Mohamed Zuki, F. B., Kheireddine Aroua, M., & Ibbora, C. V. (2019). Low-cost, biodegradable and highly effective adsorbents for batch and column fixed bed adsorption processes of methylene blue. *Journal of Environmental Chemical Engineering, 7*(5), 103409. https://doi.org/10.1016/j.jece.2019.103409

Alhashimi, H. A., & Aktas, C. B. (2017). Life cycle environmental and economic performance of biochar compared with activated carbon: A meta-analysis. *Resources, Conservation and Recycling, 118*, 13–26. https://doi.org/10.1016/j.resconrec.2016.11.016

Bayramoglu, G., Kunduzcu, G., & Arica, M. Y. (2020). Preparation and characterization of strong cation exchange terpolymer resin as effective adsorbent for removal of disperse dyes. *Polymer Engineering & Science, 60*(1), 192–201. https://doi.org/10.1002/pen.25272

Boakye, P., Tran, H. N., Lee, D. S., & Woo, S. H. (2019). Effect of water washing pretreatment on property and adsorption capacity of macroalgae-derived biochar. *Journal of Environmental Management, 233*(December 2018), 165–174. https://doi.org/10.1016/j.jenvman.2018.12.031

Cao, D. J., Wang, J. J., Zhang, Q., Wen, Y. Z., Dong, B., Liu, R. J., Yang, X., & Geng, G. (2019). Biodegradation of triphenylmethane dye crystal violet by Cedecea davisae. *Spectrochimica Acta - Part A: Molecular and Biomolecular Spectroscopy, 210*, 9–13. https://doi.org/10.1016/j.saa.2018.11.004

Chahinez, H.-O., Abdelkader, O., Leila, Y., & Tran, H. N. (2020). One-stage preparation of palm petiole-derived biochar: Characterization and application for adsorption of crystal violet dye in water. *Environmental Technology & Innovation, 19*, 100872. https://doi.org/10.1016/j.eti.2020.100872

Changmai, M., Banerjee, P., Nahar, K., & Purkait, M. K. (2018). A novel adsorbent from carrot, tomato and polyethylene terephthalate waste as a potential adsorbent for Co (II) from aqueous solution: Kinetic and equilibrium studies. *Journal of Environmental Chemical Engineering, 6*(1), 246–257. https://doi.org/10.1016/j.jece.2017.12.009

Coughlin, R. W., & Ezra, F. S. (1968). Role of surface acidity in the adsorption of organic pollutants on the surface of carbon. *Environmental Science and Technology, 2*(4), 291–297. https://doi.org/10.1021/es60016a002

Cunha, M. R., Lima, E. C., Lima, D. R., da Silva, R. S., Thue, P. S., Seliem, M. K., Sher, F., dos Reis, G. S., & Larsson, S. H. (2020). Removal of captopril pharmaceutical from synthetic pharmaceutical-industry wastewaters: Use of activated carbon derived from Butia catarinensis. *Journal of Environmental Chemical Engineering, 8*(6), 104506. https://doi.org/10.1016/j.jece.2020.104506

Fang, R. (2012). Preparation of corncob-based bio-char and its application in removing basic dyes from aqueous solution. *Advanced Materials Research, 550–553*, 2420–2423. https://doi.org/10.4028/www.scientific.net/AMR.550-553.2420

Gasmi, A., Elboughdiri, N., Ghernaout, D., Hannachi, A., Abdel Halim, K. S., & Khan, M. I. (2022). Electrocoagulation process for removing dyes and chemical oxygen demand from wastewater: operational conditions and economic assessment — a review. *DESALINATION AND WATER TREATMENT, 271*, 74–107. https://doi.org/10.5004/dwt.2022.28792

Gasmi, A., Ibrahimi, S., Elboughdiri, N., Tekaya, M. A., Ghernaout, D., Hannachi, A., Mesloub, A., Ayadi, B., & Kolsi, L. (2022). Comparative study of chemical coagulation and electrocoagulation for the treatment of real textile wastewater: Optimization and operating cost estimation. *ACS Omega, 7*(26), 22456–22476. https://doi.org/10.1021/acsomega.2c01652

Grimm, A., dos Reis, G. S., Dinh, V. M., Larsson, S. H., Mikkola, J. P., Lima, E. C., & Xiong, S. (2022). Hardwood spent mushroom substrate–based activated biochar as a sustainable bioresource for removal of emerging pollutants from wastewater. *Biomass Conversion and Biorefinery, 0123456789*, 1–17. https://doi.org/10.1007/s13399-022-02618-7

Guz, L., Curutchet, G., Torres Sánchez, R. M., & Candal, R. (2014). Adsorption of crystal violet on montmorillonite (or iron modified montmorillonite) followed by degradation through Fenton or photo-Fenton type reactions. *Journal of Environmental Chemical Engineering, 2*(4), 2344–2351. https://doi.org/10.1016/j.jece.2014.02.007

Hadj-Otmane, C., Ouakouak, A., Touahra, F., Grabi, H., Martín, J., & Bilal, M. (2022). Date palm petiole–derived biochar: effect of pyrolysis temperature and adsorption properties of hazardous cationic dye from water. *Biomass Conversion and Biorefinery., 2022*, 1–11. https://doi.org/10.1007/s13399-022-03127-3

Hu, B., Ai, Y., Jin, J., Hayat, T., Alsaedi, A., Zhuang, L., & Wang, X. (2020). Efficient elimination of organic and inorganic pollutants by biochar and biochar-based materials. *Biochar, 2*(1), 47–64. https://doi.org/10.1007/s42773-020-00044-4

Huff, M. D., & Lee, J. W. (2016). Biochar-surface oxygenation with hydrogen peroxide. *Journal of Environmental Management, 165*, 17–21. https://doi.org/10.1016/j.jenvman.2015.08.046

Khan, M. I., Shanableh, A., Elboughdiri, N., Lashari, M. H., Manzoor, S., Shahida, S., Farooq, N., Bouazzi, Y., Rejeb, S., Elleuch, Z., Kriaa, K., & ur Rehman, A. (2022). Adsorption of methyl orange from an aqueous solution onto a BPPO-based anion exchange membrane. *ACS Omega, 7*(30), 26788–26799. https://doi.org/10.1021/acsomega.2c03148

Kumi, A. G., Ibrahim, M. G., Fujii, M., & Nasr, M. (2020). Synthesis of sludge-derived biochar modified with eggshell waste for monoethylene glycol removal from aqueous solutions. *SN Applied Sciences, 2*(10), 1696. https://doi.org/10.1007/s42452-020-03501-8

Lima, D. R., Hosseini-Bandegharaei, A., Thue, P. S., Lima, E. C., de Albuquerque, Y. R. T., dos Reis, G. S., Umpierres, C. S., Dias, S. L. P., & Tran, H. N. (2019). Efficient acetaminophen removal from water and hospital effluents treatment by activated carbons derived from Brazil nutshells. *Colloids and Surfaces A: Physicochemical and Engineering Aspects, 583*(July), 123966. https://doi.org/10.1016/j.colsurfa.2019.123966

Lima, É. C., Adebayo, M. A., & Machado, F. M. (2015). Kinetic and equilibrium models of adsorption. In Carbon Nanostructures (0, 9783319188744). https://doi.org/10.1007/978-3-319-18875-1_3 33-69.Springer

Liu, W., Yuan, H., & Ke, Y. (2020). Preparation and characterization of ordered mesoporous carbon based on soybean oil. *Journal of Materials Science, 55*(15), 6525–6536. https://doi.org/10.1007/s10853-020-04480-2

Mao, X., Yan, Z., Sheng, T., Gao, M., Zhu, H., Xiao, W., & Wang, D. (2017). Characterization and adsorption properties of the electrolytic carbon derived from CO_2 conversion in molten salts. *Carbon, 111*, 162–172. https://doi.org/10.1016/j.carbon.2016.09.035

Msaadi, R., Sassi, W., Hihn, J. Y., Ammar, S., & Chehimi, M. M. (2022). Valorization of pomegranate peel balls as bioadsorbents of methylene blue in aqueous media. *Emergent Materials, 5*(2), 381–390. https://doi.org/10.1007/s42247-021-00174-w

Naima, A., Ammar, F., Abdelkader, O., Rachid, C., Lynda, H., Syafiuddin, A., & Boopathy, R. (2022). Development of a novel and efficient biochar produced from pepper stem for effective ibuprofen removal. *Bioresource Technology, 347*(November 2021), 126685. https://doi.org/10.1016/j.biortech.2022.126685

Ouakouak, A., Abdelhamid, M., Thouraya, B., Chahinez, H. O., Hocine, G., Hamdi, N., Syafiuddin, A., & Boopathy, R. (2021). Development of a novel adsorbent prepared from dredging sediment for effective removal of dye in aqueous solutions. *Applied Sciences (Switzerland), 11*(22), 10722. https://doi.org/10.3390/app112210722

Pandian, C. J., Palanivel, R., & Dhananasekaran, S. (2015). Green synthesis of nickel nanoparticles using Ocimum sanctum and their application in dye and pollutant adsorption. *Chinese Journal of Chemical Engineering, 23*(8), 1307–1315. https://doi.org/10.1016/j.cjche.2015.05.012

Pandit, N. R., Mulder, J., Hale, S. E., Zimmerman, A. R., Pandit, B. H., & Cornelissen, G. (2018). Multi-year double cropping biochar field trials in Nepal: Finding the optimal biochar dose through agronomic trials and cost-benefit analysis. *Science of The Total Environment, 637–638*, 1333–1341. https://doi.org/10.1016/j.scitotenv.2018.05.107

Praveen, S., Gokulan, R., Pushpa, T. B., & Jegan, J. (2021). Techno-economic feasibility of biochar as biosorbent for basic dye sequestration. *Journal of the Indian Chemical Society, 98*(8), 100107. https://doi.org/10.1016/j.jics.2021.100107

Rouahna, N., Barkat, D., Ouakouak, A., & Srasra, E. (2018). Synthesis and characterization of Mg-Al layered double hydroxide intercalated with D2EHPA: Application for copper ions removal from aqueous solution. *Journal of Environmental Chemical Engineering, 6*(1), 1226–1232. https://doi.org/10.1016/j.jece.2018.01.036

Sabnis, R. W. (2007). Handbook of acid-base indicators (21, 1). CRC Press. https://doi.org/10.1201/9780849382192

Sakhiya, A. K., Vijay, V. K., & Kaushal, P. (2022). Efficacy of rice straw derived biochar for removal of Pb+2 and Zn+2 from aqueous: Adsorption, thermodynamic and cost analysis. *Bioresource Technology Reports, 17*, 100920. https://doi.org/10.1016/j.biteb.2021.100920

Sevilla, M., Fuertes, A. B., & Mokaya, R. (2011). High density hydrogen storage in superactivated carbons from hydrothermally carbonized renewable organic materials. *Energy and Environmental Science, 4*(4), 1400–1410. https://doi.org/10.1039/c0ee00347f

Sewu, D. D., Lee, D. S., Tran, H. N., & Woo, S. H. (2019). Effect of bentonite-mineral co-pyrolysis with macroalgae on physicochemical property and dye uptake capacity of bentonite/biochar composite. *Journal of the Taiwan Institute of Chemical Engineers, 104*, 106–113. https://doi.org/10.1016/j.jtice.2019.08.017

Tomul, F., Arslan, Y., Başoğlu, F. T., Babuçcuoğlu, Y., & Tran, H. N. (2019). Efficient removal of anti-inflammatory from solution by Fe-containing activated carbon: Adsorption kinetics, isotherms, and thermodynamics. *Journal of Environmental Management, 238*, 296–306. https://doi.org/10.1016/j.jenvman.2019.02.088

Tran, H. N., Lee, C. K., Nguyen, T. V., & Chao, H. P. (2018). Saccharide-derived microporous spherical biochar prepared from hydrothermal carbonization and different pyrolysis temperatures: synthesis, characterization, and application in water treatment. *Environmental Technology (United Kingdom), 39*(21), 2747–2760. https://doi.org/10.1080/09593330.2017.1365941

Tran, H. N., Tomul, F., Ha, N. T. H., Nguyen, D. T., Lima, E. C., Le, G. T., Chang, C. T., Masindi, V., & Woo, S. H. (2020). Innovative spherical biochar for pharmaceutical removal from water: Insight into adsorption mechanism. *Journal of Hazardous Materials, 394*(January), 122255. https://doi.org/10.1016/j.jhazmat.2020.122255

Tran, H. N., Wang, Y. F., You, S. J., & Chao, H. P. (2017). Insights into the mechanism of cationic dye adsorption on activated charcoal: The importance of Π–Π interactions. *Process Safety and Environmental Protection, 107*, 168–180. https://doi.org/10.1016/j.psep.2017.02.010

Vo, A. T., Nguyen, V. P., Ouakouak, A., Nieva, A., Doma, B. T., Tran, H. N., & Chao, H. P. (2019). Efficient removal of Cr(VI) from water by biochar and activated carbon prepared through hydrothermal carbonization and pyrolysis: Adsorption-coupled reduction mechanism. *Water (Switzerland), 11*, 6. https://doi.org/10.3390/w11061164

Wathukarage, A., Herath, I., Iqbal, M. C. M., & Vithanage, M. (2019). Mechanistic understanding of crystal violet dye sorption by woody biochar: implications for wastewater treatment. *Environmental Geochemistry and Health, 41*(4), 1647–1661. https://doi.org/10.1007/s10653-017-0013-8

Wu, J., Yang, J., Feng, P., Huang, G., Xu, C., & Lin, B. (2020). High-efficiency removal of dyes from wastewater by fully recycling litchi peel biochar. *Chemosphere, 246*, 125734. https://doi.org/10.1016/j.chemosphere.2019.125734

Xiang, W., Zhang, X., Chen, J., Zou, W., He, F., Hu, X., Tsang, D. C. W., Ok, Y. S., & Gao, B. (2020). Biochar technology in wastewater treatment: A critical review. *Chemosphere, 252*, 126539. https://doi.org/10.1016/j.chemosphere.2020.126539

Yaseen, D. A., & Scholz, M. (2019). Textile dye wastewater characteristics and constituents of synthetic effluents: a critical review. In International Journal of Environmental Science and Technology 16, 2. Springer . https://doi.org/10.1007/s13762-018-2130-z

Yihunu, E. W., Minale, M., Abebe, S., & Limin, M. (2019). Preparation, characterization and cost analysis of activated biochar and hydrochar derived from agricultural waste: A comparative study. *SN Applied Sciences, 1*(8), 873. https://doi.org/10.1007/s42452-019-0936-z

Yu, H., Zou, W., Chen, J., Chen, H., Yu, Z., Huang, J., Tang, H., Wei, X., & Gao, B. (2019). Biochar amendment improves crop production in problem soils: A review. *Journal of Environmental Management, 232*(May 2018), 8–21. https://doi.org/10.1016/j.jenvman.2018.10.117

Zbair, M., Anfar, Z., Khallok, H., Ahsaine, H. A., Ezahri, M., & Elalem, N. (2018). Adsorption kinetics and surface modeling of aqueous methylene blue onto activated carbonaceous wood sawdust. *Fullerenes Nanotubes and Carbon Nanostructures, 26*(7), 433–442. https://doi.org/10.1080/1536383X.2018.1447564

Zubair, M., Muazu, N. D., Jarrah, N., Blaisi, N. I., Aziz, H. A., & Al-Harthi, M. (2020). Adsorption behavior and mechanism of methylene blue, crystal violet, eriochrome black T, and methyl orange dyes onto biochar-derived date palm fronds waste produced at different pyrolysis conditions. *Water, Air, & Soil Pollution, 231*(5), 240. https://doi.org/10.1007/s11270-020-04595-x